Journal of Studies in Science and Engineering

EngiScience Publisher

*Research Article*

# Cogging Torque Reduction of Brushless DC Motor: Investigating the Efficacy of Radial Pole Shaping Technique with Novel Bump-Shaped Rotor Pole

**Tanuj Jhankal [1], Amit N. Patel [1,*]**

[1] Department of Electrical Engineering, Institute of Technology, Nirma University, Ahmadabad, 382481, India

*Corresponding Author: Amit N. Patel, E-mail: amit.patel@nirmauni.ac.in

**Article Info**

Article History

Received: Feb 12, 2024

Revised: Apr 09, 2024

Accepted: Apr 15, 2024

**Keywords**

Cogging Torque

Torque Ripple

Brushless DC Motor

Low-Speed Application

Finite Element Analysis

**Abstract**

With the rising demand for high-performance motors in electrical vehicle applications, permanent magnet brushless DC motors are a promising solution due to their various attractive features. However, it has a significant drawback of high cogging torque, which deteriorates the overall motor performance. This negative impact is dominating in electric vehicles for low-speed applications. It is desirable to reduce the cogging torque to improve the performance of the radial flux brushless DC motor. The prime focus of this research is reducing cogging torque through the radial pole shaping technique with a bump-shaped rotor pole surface. This work also investigates the impact of the proposed approach on torque ripple and motor performance while cutting down the requirement for rare earth material. This paper uses two ratings: 1000 W, 510 rpm, and 250 W, 150 rpm motors. Two reference motors of proposed ratings were designed using radial-shaped permanent magnet poles. Finite element software is used for the simulation and modeling of the motors. A novel bump-shaped permanent magnet pole shape is introduced, and in-depth investigations have been carried out to evaluate the impact of the proposed pole shape on cogging torque. The validity of the analysis results is further substantiated by comparing the improved and reference model results. The comparison investigation indicates that the motor equipped with the proposed pole shape performs better than the reference motor.



## 1. Introduction

The growing need for eco-friendly and energy-efficient transportation to reduce carbon emissions from the transportation industry is driving up demand for electric vehicles (EVs) [1-3]. Due to the ongoing global energy crisis, scientists and researchers have been encouraged to develop environmentally friendly modes of transportation with no emissions. Hence, the selection of the motor topology is crucial as it considerably impacts the performance of the entire EV [4]. A permanent magnet brushless DC (BLDC) motor is a promising solution. This is because of its attractive features, such as outstanding efficiency, compact design, good dynamic response, dependable performance, high power density, and low noise [5-8]. Brushless DC motors use rare earth permanent magnet (REPM) material to bolster the performance, unlike

conventional motors, which rely on electric stimulation. The Utilization of REPM material reduces copper loss and enhances the magnetic flux, which results in higher performance than conventional motors. Brushless DC motors employ various permanent magnet types, i.e., Neodymium-Iron-Boron (NdFeB), Samarium Cobalt (Sm-Co), AlNiCo, and Ferrites. NdFeB and SM-Co are classified as REPM materials in all the magnets used. Neodymium-Iron-Boron REPM material is considered the best available grade because of its highest energy product and higher magnetic flux, allowing the designing of more compact-sized motors compared to that with AlNico or Ferrite magnets [9, 10].

Permanent magnet orientation and magnetic flux arrangement are used to categorise BLDC motors into various categories. Based on permanent magnet placement, permanent magnet (PM) motors are classified into three classes, i.e., surface PM, inset PM, and interior PM. Based on flux flow, PM motors are categorized into radial flux, axial flux, and transverse flux PM motors. This work focuses on surface permanent magnet radial flux class BLDC (SPM-RFBLDC) motor. It has improved power transmission, fast acceleration and deceleration, reduced energy losses, and, most importantly, simpler contraction compared to other topologies. Every motor topology has benefits and drawbacks, making them ideal for different uses. Hence, before considering any motor topology, it is crucial to carefully assess the application's specific requirements and weigh each motor type's advantages and disadvantages.

Understanding the importance of torque quality, a critical factor in motor performance. Alongside efficiency and size, torque quality plays a significant role. The pursuit of superior torque quality while meeting the required torque is always a worthwhile endeavor. The performance of the SPM-RFBLDC motor can be profoundly impacted by a high torque ripple (TR), which introduces unwelcome noise and vibrations. Therefore, achieving a low TR enhances performance and torque quality. The primary culprits behind TR are cogging torque (CT), harmonic components in back-electromotive force, and magnetic circuit saturation. CT, a significant contributor to TR, results from the interplay between air-gap reluctance change and MMF due to PM in the motor. While cogging torque does not directly generate torque, it amplifies the TR by overlaying the motor's torque profile. To reduce TR and improve torque quality, it is crucial to minimise CT. This can be achieved through design side variations or control side modifications. In high-speed applications, torque ripple is mitigated by the system's moment of inertia, but in low-speed applications, TR leads to undesirable motor vibration and noise. Therefore, minimising CT is essential to reduce torque fluctuation and enhance the overall quality of the motor's torque output. There are two main approaches to CT reduction in PM motors: design-based and control-based [11]. CT is reduced by modifying and optimising motor design parameters using the design side approach.

Regarding reducing CT, the control side approach relies heavily on precise current excitation and the reliability and accuracy of sensors. However, design-oriented approaches have proven more effective, instilling confidence in their potential. Approaches such as magnet shifting, stator skewing, rotor skewing,

step skewing, the combination of slots poles, slot opening variation, segmented stator laminations, unequal placement of rotor magnets, and the addition of dummy slots and notching have shown promise in reducing CT [12-17]. Skewing, a widely accepted technique in the industry [18], is a commonly used method. Many researchers have been diligently investigating the field of CT reduction through these strategies. Several literary works have suggested the implementation of an asymmetrical pole shaping methodology [19] and the incorporation of a Herringbone design arrangement, in addition to the usual skewing method, to address the issue of axial force imbalance [20].

This paper emphasizes the minimization of CT of the SPM-RFBLDC motor using a novel REPM pole design. When utilizing the proposed REPM shape to get the desired outcomes, it is always desirable to either reduce the REPM material weight or keep it constant. As most researchers aim to diminish torque fluctuations with reduced CT and achieve improved performance at a lower cost of permanent magnets, the proposed bump-shaped REPM pole design in SPM-RFBLDC motors can reduce CT and improve the torque profile. The proposed bump-shaped pole-shaping technique offers a distinct advantage over these traditional methods, i.e., skewing and magnet shifting. By strategically designing the pole shape, we mitigate cogging torque and reduce the required permanent magnet material without introducing additional axial thrust to the motor. This results in potential cost savings and contributes to sustainability by minimizing material usage. The proposed bump-shaped configuration is realized by changing the pole shape radially. Electromagnetic analysis is performed on every configured design. After the electromagnetic analysis, it was determined that the SPM-RFBLDC rotor design featuring a permanent magnet pole in a bump-shaped configuration exhibits superior electromagnetic performance in reducing CT. The flow of the paper is as follows: The design of the reference SPM-RFBLDC motor is presented in section 2. Section 3 discusses the performance parameters. The effectiveness of the proposed REPM rotor pole topology is validated by comparing the results with the reference model in Section 4, while the conclusion is drawn in Section 5.

## 2. Design of Reference SPM-RFBLDC Motors

Two different ratings 3-phase reference SPM-RFBLDC motors are designed using radial-shaped rotor poles. Figure 1 illustrates the 2-D and 3-D views of the SPM-RFBLDC motor. Where $L$ is the motor length, $D_{so}$ is the stator outer diameter or motor diameter, $D_{ri}$ and $D_{ro}$ are the rotor inner and outer diameter, respectively, Lm is the magnet length, $w_{sc}$ is the width of the stator core, and $w_{rc}$ is the width of the rotor core. Designing an SPM-RFBLDC motor requires some basic parameters to be selected, including electric loading, magnetic loading, sizing constraints, current density, material for core and permanent magnet poles, slot-pole combination, and winding type [21]. Both motors are designed to consider the current density range between 5 - 12 A/mm$^2$ in this design process. Neodymium Iron Boron material is employed in

designing the rotor poles, while M19 electrical steel material of 29 grade is utilized for stator teeth and stator and rotor core. Figure 2 represents the developed reference models of 1000 W, 510 rpm, and 250 W, 150 rpm ratings SPM-RFBLDC motor with radial pole shape.

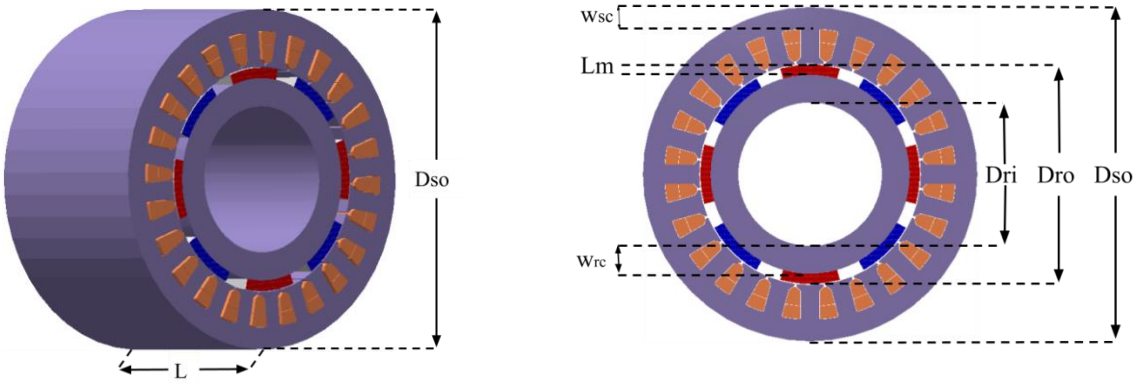


(a) 3-D view (b) 2-D view

**Figure 1.** 2-D and 3-D constructional view of SPM-RFBLDC motor.

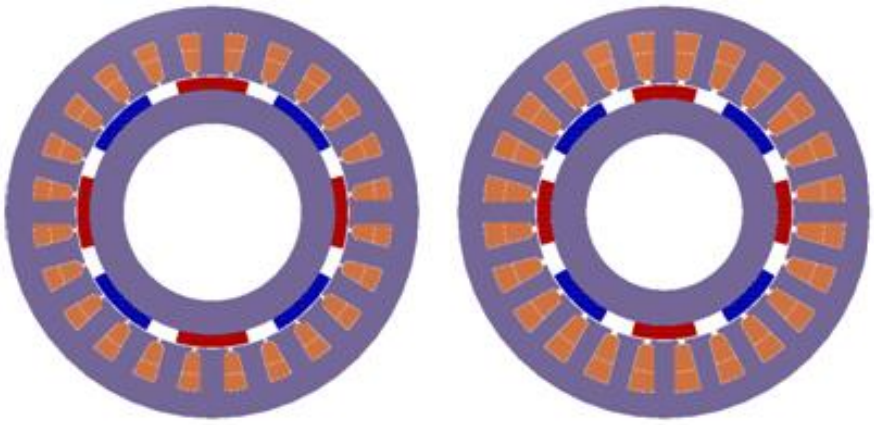

(a) (b)

**Figure 2.** Developed finite element models of three different ratings: (a) 1000 W and (b) 250 W.

Figure 3 depicts the whole design process with a reference performance comparison and improves the SPM-RFBLDC motor. The developed design program is a five-stage process. Firstly, the motor's specifications (i.e., power ($P$), speed ($\omega$), supply voltage ($V$), number of poles ($N_p$), and number of slots ($N_s$)) are provided along with the initial assumptions of various parameters (i.e., current density ($\delta$), length of air-gap ($l_g$), materials, type of winding, aspect ratio, split ratio, electric and magnetic loading, etc.). In the second stage, stator design is carried out, after which the rotor design is carried out in stage third. In the fourth stage, a performance calculation is carried out using the design motor. Now, the performance is compared with the desired performance in stage five. If the performance is as desired, the design will stop. Otherwise, stage 5 will return the program to the rotor design stage with a change in rotor pole shape. The main design specifications and ratings of the reference designs are listed in Table 1.

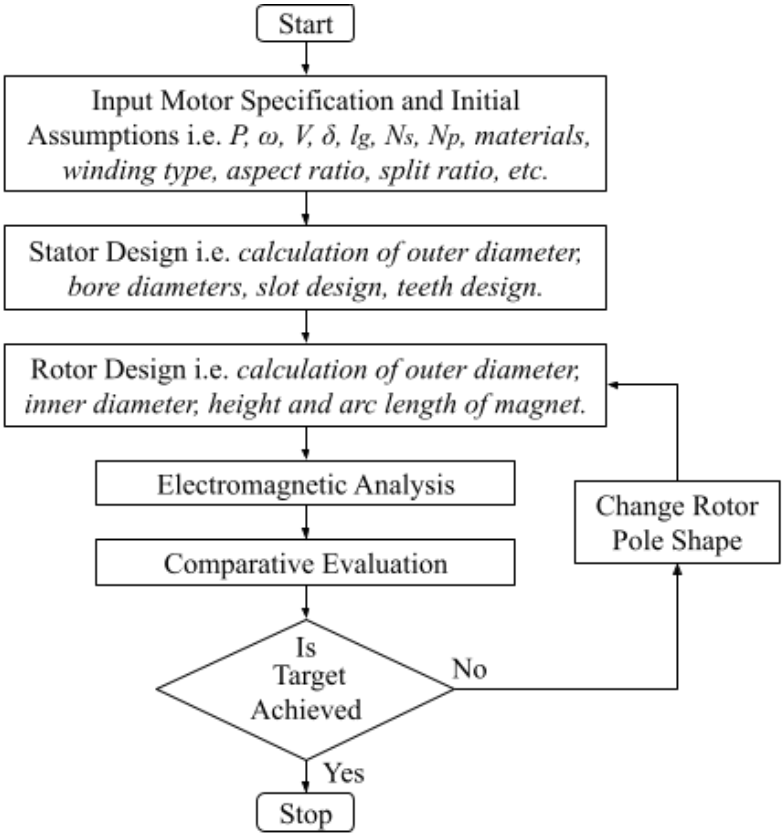


**Figure 3.** Design process of SPM-RFBLDC motors [22].

**Table 1.** Ratings and main design specifications of reference motors

| **Parameter** | **Unit** | **Motor 1** | **Motor 2** |
|---|---|---|---|
| Rated Power | W | 1000 | 250 |
| Rated Speed | rpm | 510 | 150 |
| Rated Torque | N.m. | 18.7 | 15.8 |
| Supply Voltage | volts | 48 | 48 |
| No. of slots | - | 24 | 24 |
| No. of poles | - | 8 | 8 |
| Motor Diameter | mm | 163 | 145.6 |
| Motor length | mm | 95.7 | 101.9 |
| Length of air-gap | mm | 0.5 | 0.5 |
| Magnet fraction | - | 0.7 | 0.67 |
| Fill factor (%) | - | 40 | 40 |
| Slots/pole/phase | - | 1 | 1 |
| Permanent magnet pole height | mm | 5 | 5 |
| Core material | - | M19 - 29Ga | M19 - 29Ga |
| Permanent magnet material | - | NdFeB - N38 | NdFeB - N40 |

In the improved design with the proposed pole shape, the stator is kept unchanged as a reference design, and the rotor side is changed by only changing the pole shape from radial to the proposed one, as displayed in Figure 4. Figure 4 also displays the various parameters (i.e., $h_{arc}$ is the height of the bump arc, $l_{arc}$ is the length of the bump arc, $h_{m'}$ is the new height of the magnet excluding the height of the bump and $\theta_m$ is the magnet pole arc) which plays a vital role in the selection of optimal bump shape for the two different SPM-RFBLDC motors as the calculation of bump radius is directly depending on these parameters.

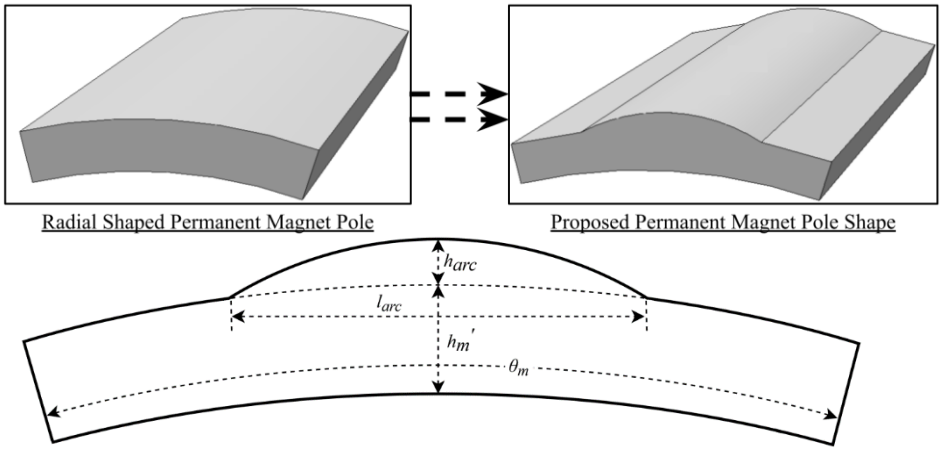


**Figure 4.** Proposed bump-shaped permanent magnet pole structure for SPM-RFBLDC motor.

## 3. Electromagnetic Analysis

Evaluation and comparative analysis reference and proposed designs for both 1000 W and 250 W motors are presented in this section. Electromagnetic analysis assesses different performance parameters, i.e., weight, efficiency, back EMF, flux density, CT, and torque.

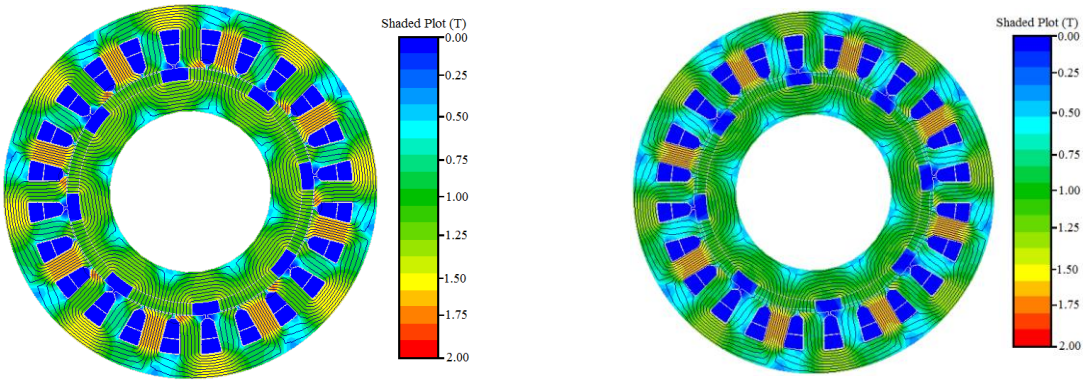


(a) (b)

**Figure 5.** Flux density plot of 1000 W, 510 rpm motor (a) reference motor and (b) motor with the proposed bump-shaped pole.

The flux density plots of 1000 W and 250 W SPM-RFBLDC reference and improved motors are obtained using finite element analysis (FEA). Figure 5 and Figure 6 show the comparison of flux density plots of 1000 W and 250 W SPM-RFBLDC motors with reference radial type poles and proposed pole shapes, respectively. The flux density analysis shows that the measured flux density closely matches the assumed flux density in different motor sections. No saturation is observed since the flux density remains within the permissible limit for all the models (i.e., 1.3-1.7 T).

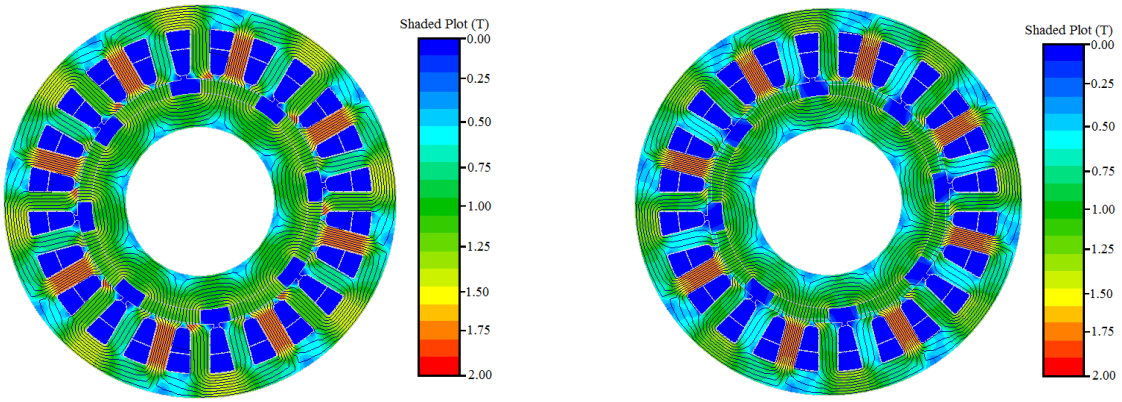


(a) (b)

**Figure 6.** Flux density plot of 250 W, 150 rpm motor (a) reference motor and (b) motor with the proposed bump-shaped pole.

### 3.1. Cogging Torque

Cogging torque represents a fundamental characteristic of SPM-RFBLDC motors, stemming from the interaction between the permanent magnet poles on the rotor's side and the stator teeth in SPM-RFBLDC motors. Within SPM-RFBLDC motors, the stator teeth serve as the primary source of reluctance variation, while the primary cause of magnetic flux fluctuation is attributed to the permanent magnet poles. Remarkably, CT is observable without a power supply to the stator windings. It is most visible at low speed, with the symptoms of jerks and noise. At high speed, the moment of inertia of the motor filters out jerks and vibration due to CT. This torque exhibits periodic behavior due to the cyclical changes in air-gap reluctance. The expression for CT is represented as [23, 24, 25, 26].

$$T_{cogg.} = -\frac{\partial W}{\partial \theta} \tag{1}$$

Here, $W$ symbolises the energy of the magnetic field, and $\theta$ indicates the rotation angle. The expression for the stored magnetic-field energy in SPM-RFBLDC motors can be stated as shown in Eq. (2), assuming the radial edge effects are neglected.

$$W \cong W_{magnet+air-gap} \tag{2}$$

$$W = \frac{\int_V Q_0 B_\alpha^2(\beta) dV}{2\mu_0} \tag{3}$$

$$Q(\beta, \theta) = \left( \frac{h_m(\beta)}{h_m(\beta) + \delta(\beta, \theta)} \right)^2 \tag{4}$$

Here $Q(\beta, \theta)$ is air-gap relative permeance, $\mu_0$ is free space permeability, $V$ is the volume of air-gap, $\beta$ is the circumference angle of air-gap, $B_\alpha(\beta)$ is distribution of flux density in the air-gap, $\delta(\beta, \theta)$ is the distribution function of effective air-gap length and $h_m$ height of the PM,. The $B_\alpha^2$ and $C$ expressions are

$$B_\alpha^2(\beta) = B_{\alpha\beta} + \sum_{z=1}^{\infty} B_{\alpha z} \cos(2zp\beta) \tag{5}$$

and

$$Q = Q_0 + \sum_{z=1}^{\infty} Q_z \cos\big(jz(\beta + \theta)\big) \tag{6}$$

Re-writing Eq. (1) by using Eqs. (2) to (6), $T_{cogg}$. is expressed as,

$$T_{cogg.}(\theta) = \frac{\pi z \delta (R_{sout}^2 - R_{rc}^2)}{4\mu_0} \sum_{z=1}^{\infty} z Q_z \, B_{\alpha z U/2p} \sin(zK\theta) \tag{7}$$

Where, $K$ is the least common multiple of the number of poles and number of stator slots, $p$ is the number of pole-pairs, number of stator slots is represented by $N_s$, $R_{sout}$ is the stator's outer radius, $R_{rc}$ is the rotor core radius, $Q_0$ and $Q_z$ are the Fourier series coefficients. As with the change in PM pole shape, it leads to the change in $C(\beta + \theta)$ and $B_\alpha(\beta)$. Hence, this changes the magnetic field energy stored, which leads to a change in the motor's CT, as shown in Eq. (7).

Figure 7 and Figure 8 compare CT profiles obtained from the electromagnetic analysis of the model improved with the proposed pole shape for different values of bump radius (BR) and the reference model. Peak-to-peak CT of reference 1000 W and 250 W motors are 9.660 N.m. and 5.40 N.m. Keeping all the other parameters of the rotor and stator side unchanged, only bump-shaped PM-RPs are introduced instead of radial-shaped PM-RPs. To reduce the CT further, the radius of the bump arc shape varies from 0 to 20 mm for the 1000 W motor and from 0 to 19 mm for the 250 W motor. The desired result of the proposed technique is obtained at 20 mm and 19 mm bump arc radius for 1000 W and 250 W motors, respectively. In Figure 7, the reduction in CT is observed from 9.66 N.m. to 0.886 N.m. when BR is kept at 20 mm in a 1000 W motor. Moreover, CT is reduced from 5.40 N.m. to 2.926 N.m. when BR is 19 mm in a 250 W motor.

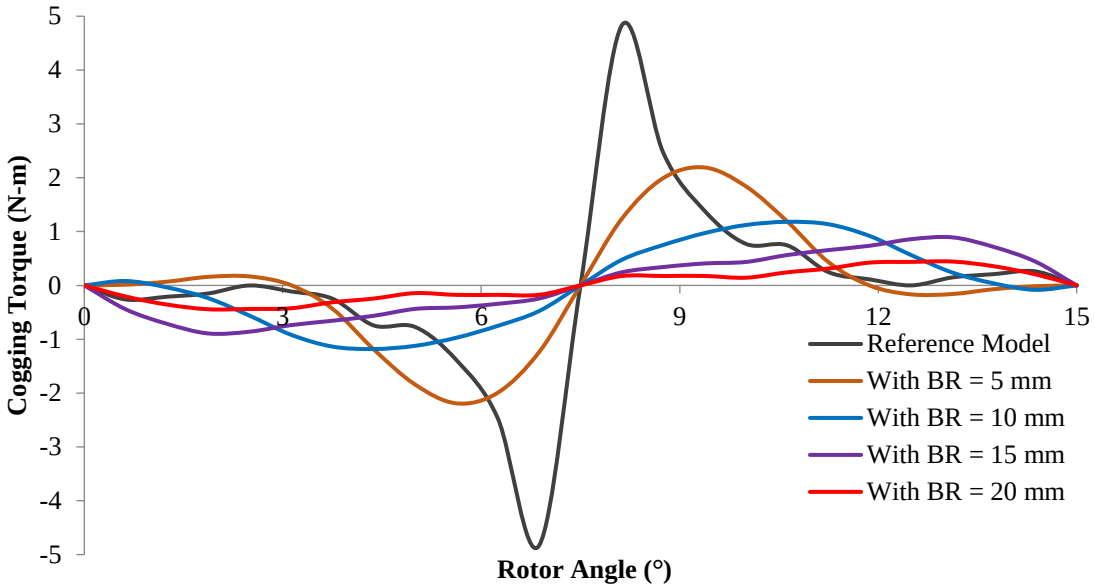


**Figure 7.** Comparison of CT profiles of 1000 W, 510 rpm motor.

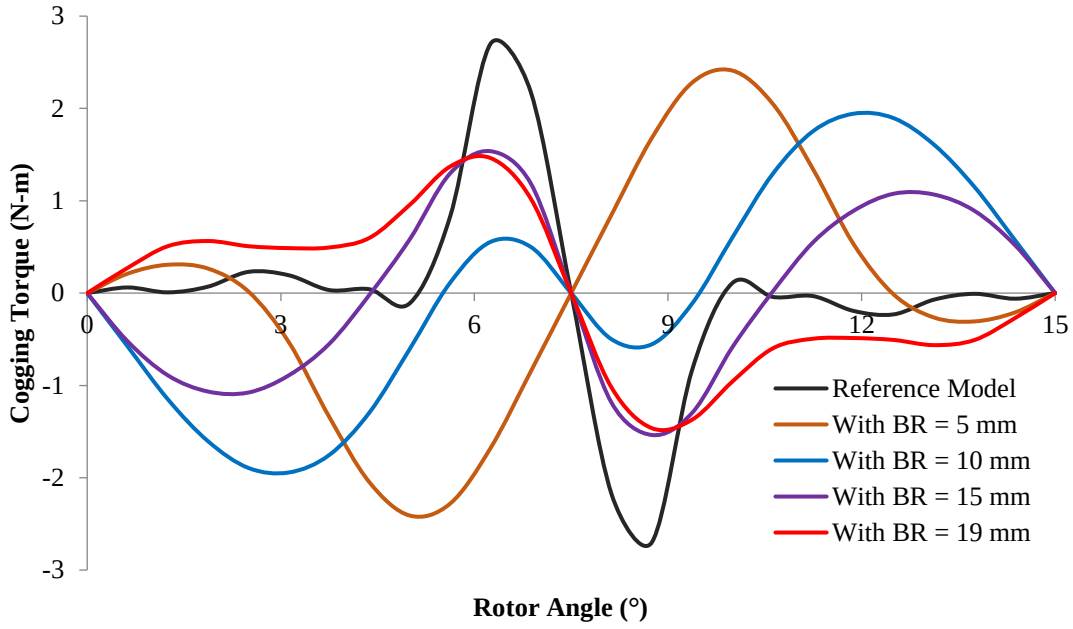


**Figure 8.** Comparison of CT profiles of 250 W, 150 rpm motor.

### 3.2. Average Torque

Here, the torque produced by the 250 W, 150 rpm, and 1000 W, 510 rpm rating motors are analyzed and investigated for reference and improved models with the proposed approach. The torque profile of 1000 W and 250 W motors designed using the radial-shaped REPM material pole (reference model) and proposed bump-shaped REPM material pole are compared and presented in Figure 9 and Figure 10, respectively. The average torque developed by the reference model of 1000 W and 250 W rating motor is 18.80 N.m. and 15.91 N.m., respectively. In contrast, the models designed using the proposed approach for reducing CT

develop an average torque of 16.6 N.m. in a 1000 W rating motor and 15.1 N.m. in a 250 W rating motor. Eq. (8) illustrates the relation for calculating TR in the torque profile. Where $T_{max}$ and $T_{min}$ are the maximum and minimum torque observed in the torque profile, and $T_{avg}$ is the average torque developed by the motor.

$$T_{ripple}(\%) = \frac{T_{max} - T_{min}}{T_{avg}} \times 100 \quad (8)$$

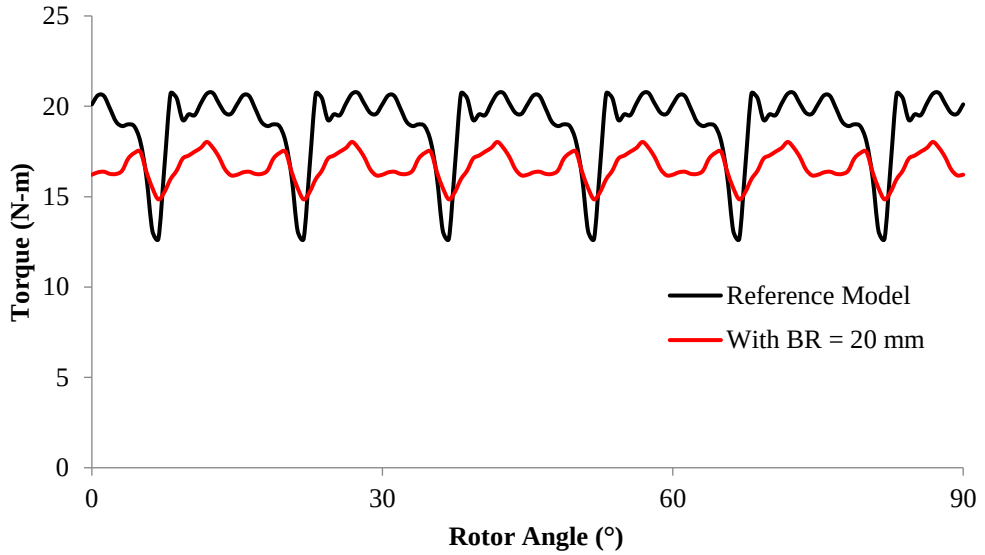


**Figure 9.** Comparison of torque profiles of reference and improved 1000 W, 510 rpm motors.

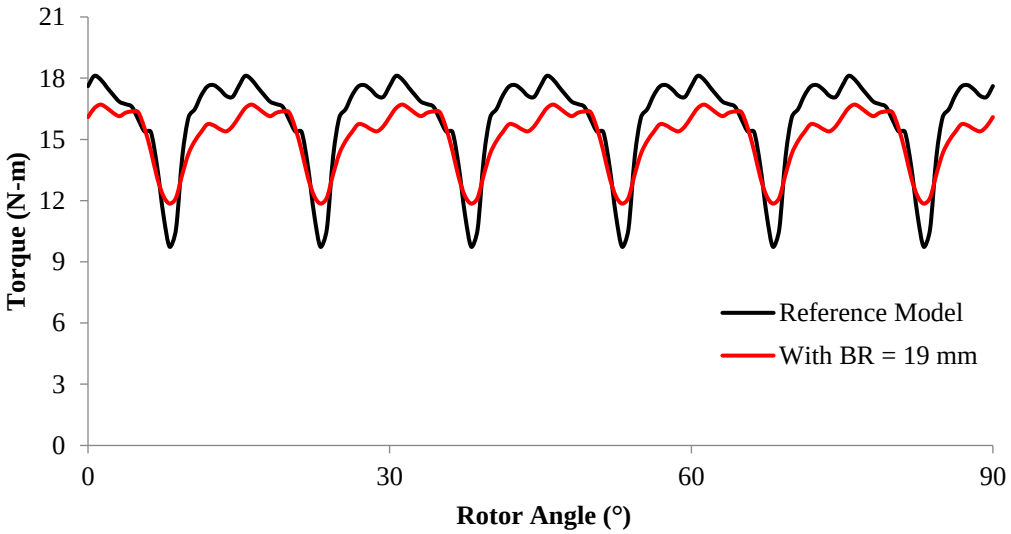


**Figure 10.** Comparison of torque profiles of reference and improved 250 W, 150 rpm motors.

### 3.3. Back - EMF

When in any coil, there is a change in flux linkage, which leads to the generation of a force known as electromotive force (EMF). Hence, it can be explained as a change in flux w.r.t. time. Back-EMF and torque are directly related in the case of SPM-RFBLDC motors. Hence, any change in either one is directly

reflected in another parameter. Figure 11 compares back-EMF profiles of improved and reference motors as a function of rotation angle. With the application of the proposed REPM pole shape, a slight reduction in the peak value of back-EMF is observed with an improved back-EMF profile with reduced harmonics. Figure 12 compares the amplitude of harmonics components present in improved and reference motor's back-EMF profiles.

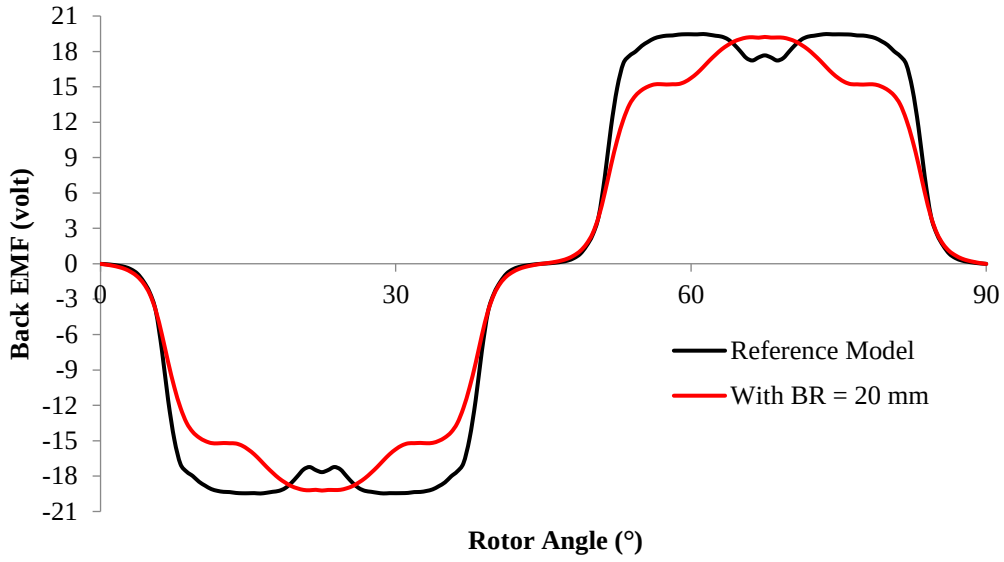


(a)

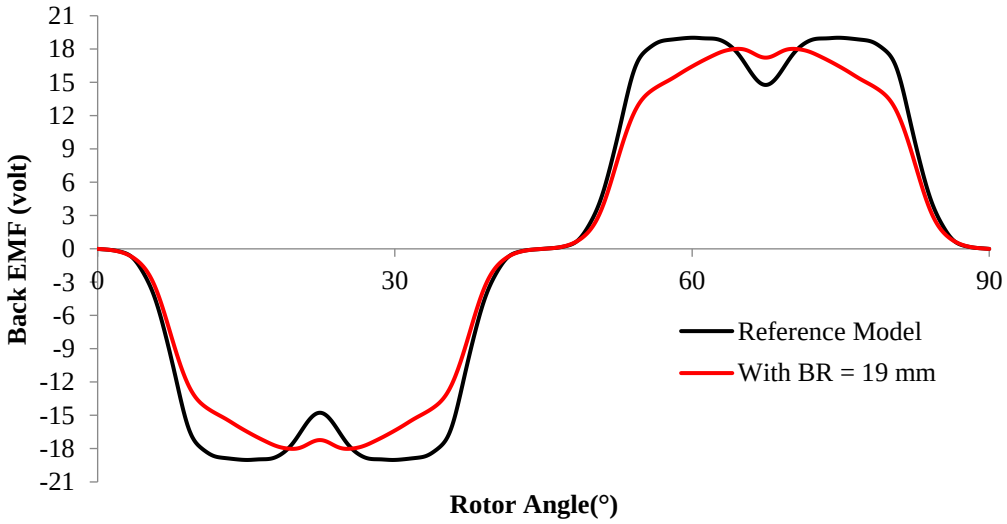


(b)

**Figure 11.** Comparison of back EMF profiles of reference and improved models (a) 1000 W, 510 rpm motor and (b) 250 W, 150 rpm motor.

The total harmonics distortion (THD) value represents the distortion caused by the presence of harmonics components in the back-EMF profile. Hence, the higher the value of THD, the higher the distortion, affecting torque quality and overall motor performance.

$$\mathrm{THD}(\%) = \frac{\sqrt{\sum_{j=2}^{n} Z_j^2}}{Z_1} \times 100 \tag{9}$$

Where $Z_j$, j and $Z_1$ represents the harmonic elements, total elements, and first-order elements, respectively.

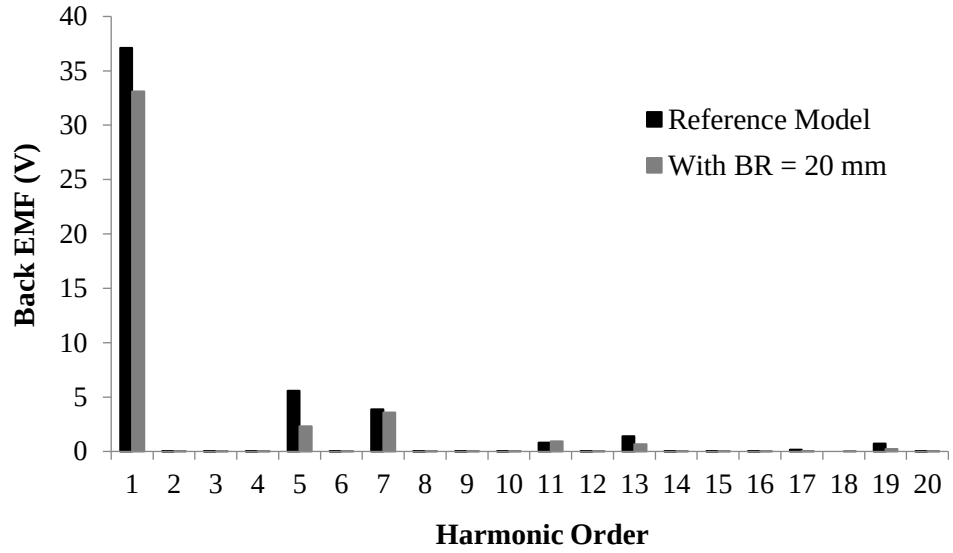


(a)

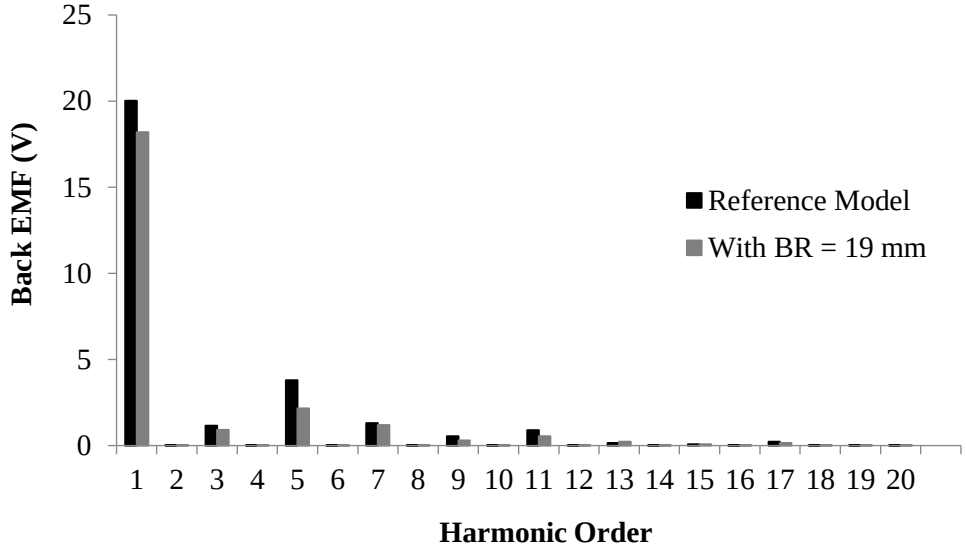


(b)

**Figure 12.** Harmonic components of back EMF profiles of reference and improved models (a) 1000 W, 510 rpm motor and (b) 250 W, 150 rpm motor.

## 4. Performance Comparison

This section compares the performance of the reference motor with a radial pole shape and the improved motor with the proposed bump shape for both ratings. A comparison of performance parameters is presented in Table 2 for both ratings.

**Table 2.** Performance comparison of reference and improved motors.

| Parameter | Unit | 1000 W, 510 rpm Motor | | 250 W, 150 rpm Motor | |
|---|---|---|---|---|---|
| | | **Reference** | **Improved** | **Reference** | **Improved** |
| Torque (T) | N.m. | 18.80 | 16.60 | 15.91 | 15.10 |
| Cogging torque(p-p) | N.m. | 9.660 | 0.886 | 5.400 | 2.926 |
| Torque ripple (%) | - | 42.85 | 19.12 | 52.63 | 32.14 |
| Power | W | 1000 | 1000 | 250 | 250 |
| Back EMF THD (%) | - | 21.84 | 13.89 | 21.56 | 14.87 |
| Overall Efficiency (%) | - | 90.3 | 89.3 | 81.7 | 80.6 |
| PM weight (Wpm) | kg | 0.805 | 0.698 | 0.680 | 0.603 |
| Motor weight | kg | 11.413 | 11.301 | 9.861 | 9.784 |
| T/Wpm Ratio | N.m./kg | 23.35 | 23.78 | 27.81 | 25.04 |

The permanent magnet weight with the proposed pole shape application is reduced from 0.805 kg and 0.680 kg to 0.698 kg and 0.603 kg in the 1000 W and 250 W designs, respectively. The torque profile is also improved in both rating designs as TR is reduced from 42.80 % to 19.12 % in the 1000 W design, whereas it is reduced from 52.63 % to 32.14 % in the 250 W design with the application of the proposed pole shape. Different performance parameters such as power, permanent magnet weight, back-EMF THD, average torque, motor overall weight, CT, and torque to permanent magnet weight ratio are also analyzed for all the designs. The proposed bump-shaped permanent magnet pole approach has shown a significant reduction in cogging torque and reduced torque ripple, leading to the improved torque characteristics of the motors. With better torque characteristics, the reliability and durability of the motor will be better. Hence, the proposed approach is favorable regarding the motor's reliability and durability in real-world applications.

## 5. Conclusion

Two 3-phase SPM-RFBLDC motors with power ratings of 1000 W and 250 W are designed with rated speeds of 510 rpm and 150 rpm, respectively. Performance analysis of the reference motors was carried out using commercially available FEA software. A novel rotor pole shape is proposed, analyzed, and compared with the reference radial-shaped pole configuration. Compared to the reference designs, the proposed approach decreases the CT with less permanent magnet material requirement. The proposed approach significantly reduces peak-to-peak CT compared to the reference motors for both ratings, i.e., 90.82 % in the 1000 W motor and 45.81 % in the 250 W rating motor. The reduction in rare earth material requirement observed with the application of the proposed pole shape is 13.29 % and 11.32 % reduction in overall rare

earth material weight in 1000 W, 510 rpm motor and 250 W, 150 rpm motor, respectively. This research unequivocally shows the efficacy of the proposed approach in CT and TR reduction with a significant reduction in rare earth material requirement. Nevertheless, the approach has its advantages and constraints. Hence, the proposed approach can be a viable option for reducing CT in other electrical motor topologies.

**Declaration of Competing Interest:** The authors declare they have no known competing interests.

## References

[1] M. F. C. Mushid and D. G. Dorrell, "Review of axial flux induction motor for automotive applications," in *2017 IEEE Workshop on Electrical Machines Design, Control and Diagnosis (WEMDCD)*, Nottingham, UK, 2017, pp. 146-151.

[2] J. A. Sanguesa, V. Torres-Sanz, P. Garrido, F. J. Martinez, and J. M. Marquez-Barja, "A review on electric vehicles: Technologies and challenges," *Smart Cities*, vol. 4, no. 1, pp. 372-404, 2021.

[3] S. Aggarwal and A. K. Singh, "Electric vehicles the future of transportation sector: a review," *Energy Sources, Part A: Recovery, Utilization, and Environmental Effects*, vol. 1, no. 0, pp. 1-21, 2021.

[4] Z. Cao, A. Mahmoudi, S. Kahourzade, and W. L. Soong, "An overview of electric motors for electric vehicles," in *31st Australasian Universities Power Engineering Conference (AUPEC)*, Perth, Australia, 2021, pp. 1-6.

[5] R. Krishnan, *Permanent Magnet Synchronous and Brushless DC Motor Drives*. CRC Press, London, UK, 2010.

[6] D. Mohanraj, J. Gopalakrishnan, B. Chokkalingam, and L. Mihet-Popa, "Critical aspects of electric motor drive controllers and mitigation of torque ripple—review," *IEEE Access*, vol. 10, pp. 73635-73674, 2022.

[7] R. Tarvirdilu, R. Zeinali, and H. B. Ertan, "An approach for performance prediction of saturated brushed permanent magnet direct current (DC) motor from physical dimensions," *Turkish Journal of Electrical Engineering and Computer Sciences*, vol. 30, no. 1, pp. 9, 2022.

[8] E. Yesilbag, Y. Ertugrul, and L. Ergene, "Axial flux PM BLDC motor design methodology and comparison with a radial flux PM BLDC motor," *Turkish Journal of Electrical Engineering and Computer Sciences*, vol. 25, no. 4, pp. 73, 2017.

[9] J. R. Miller and T. J. E. Miller, *Handershot Jr. Design of Permanent Magnet Motor*. Oxford University Press, Oxford, UK, 1994.

[10] D. C. Hanselman, *Brushless Permanent Magnet Motor Design*. McGraw-Hill, NY, USA, 1994.

[11] H. Jia, M. Cheng, W. Hua, W. Zhao, and W. Li, "Torque ripple suppression in flux-switching PM motor by harmonic current injection based on voltage space-vector modulation," *IEEE Transactions on Magnetics*, vol. 46, no. 6, pp. 1527-1530, 2010.

[12] S. M. Hwang, J. B. Eom, G. B. Hwang, W. B. Jeong, and Y. H. Jung, "Cogging torque and acoustic noise reduction in permanent magnet motors by teeth pairing," *IEEE Transactions on Magnetics*, vol. 36, no. 5, pp. 3144-3146, 2000.

[13] H. Feng, S. Zhang, J. Wei, X. Xu, C. Gao, and L. Ai, "Torque ripple reduction of brushless DC motor with convex arc-type permanent magnets based on robust optimization design," *IET Electric Power Applications*, vol. 16, no. 5, pp. 565-574, 2022.

[14] M. Aydin, Z. Q. Zhu, T. A. Lipo, and D. Howe, "Minimization of cogging torque in axial-flux permanent-magnet machines: Design concepts," *IEEE Transactions on Magnetics*, vol. 43, no. 9, pp. 3614-3622, 2007.

[15] F. Caricchi, F. G. Capponi, F. Crescimbini, and L. Solero, "Experimental study on reducing cogging torque and no-load power loss in axial-flux permanent-magnet machines with slotted winding," *IEEE Transactions on Industry Applications*, vol. 40, no. 4, pp. 1066-1075, 2004.

[16] M. Barcaro and N. Bianchi, "Torque ripple reduction in fractional-slot interior PM machines optimizing the flux-barrier geometries," in *2012 XXth International Conference on Electrical Machines*, Marseille, France, 2012, pp. 1496-1502.

[17] E. Hüner and A. Mutlu, "A new hybrid method for reducing cogging torque in the AFPM wind generator," *Energy Sources, Part A: Recovery, Utilization, and Environmental Effects*, vol. 44, no. 1, pp. 853-870, 2022.

[18] N. Bianchi and S. Bolognani, "Design techniques for reducing the cogging torque in surface-mounted PM motors," *IEEE Transactions on Industry Applications*, vol. 38, no. 5, pp. 1259-1265, 2002.

[19] Y. H. Jung, M. S. Lim, M. H. Yoon, J. S. Jeong, and J. P. Hong, "Torque ripple reduction of IPMSM applying asymmetric rotor shape under certain load condition," *IEEE Transactions on Energy Conversion*, vol. 33, no. 1, pp. 333-340, 2018.

[20] J. Liang, A. Parsapour, Z. Yang, C. Caicedo-Narvaez, M. Moallem, and B. Fahimi, "Optimization of air-gap profile in interior permanent-magnet synchronous motors for torque ripple mitigation," *IEEE Transactions on Transportation Electrification*, vol. 5, no. 1, pp. 118-125, 2019.

[21] T. Jhankal and A. N. Patel, "Design and analysis of spoke type radial flux interior permanent magnet synchronous motor for high-speed application," in *2nd Odisha International Conference on Electrical Power Engineering, Communication and Computing Technology (ODICON)*, Odisha, India, 2022, pp. 1-5.

[22] T. Jhankal and A. N. Patel, "Design and cogging torque reduction of radial flux brushless DC motors with varied permanent magnet pole shapes for electric vehicle application," *Transactions on Energy Systems and Engineering Applications*, vol. 4, no. 2, pp. 1-13, 2023.

[23] L. Zhu, S. Z. Jiang, Z. Q. Zhu, and C. C. Chan, "Analytical methods for minimizing cogging torque in permanent-magnet machines," *IEEE Transactions on Magnetics*, vol. 45, no. 4, pp. 2023-2031, 2009.

[24] X. Wang, Y. Yang, and D. Fu, "Study of cogging torque in surface-mounted permanent magnet motors with energy method," *Journal of Magnetism and Magnetic Materials*, vol. 267, no. 1, pp. 80-85, 2003.

[25] T. Jhankal and A. N. Patel, "Cogging torque minimization of high-speed spoke-type radial flux permanent magnet brushless DC motor using core bridge width variation technique," in *2023 International Conference on Recent Advances in Electrical, Electronics & Digital Healthcare Technologies (REEDCON)*, Delhi, India, 2023, pp. 750-755.

[26] D. Wang, X. Wang, M. K. Kim, and S. Y. Jung, "Integrated optimization of two design techniques for cogging torque reduction combined with analytical method by a simple gradient descent method," *IEEE Transactions on Magnetics*, vol. 48, no. 8, pp. 2265-2276, 2012.